General characterization of partially oriented polar molecules by the time-frequency profile of high-order harmonic generation

Ngoc-Loan Phan [1,2,*] Kim-Ngan H. Nguyen [1] Cam-Tu Le [3,4,†] DinhDuy Vu [1] Khang Tran,[1] and Van-Hoang Le [1,2]

[1]*Computational Physics Laboratory K002, Ho Chi Minh City University of Education, Ho Chi Minh City 70000, Vietnam*

[2]*Department of Physics, Ho Chi Minh City University of Education, Ho Chi Minh City 70000, Vietnam*

[3]*Atomic Molecular and Optical Physics Research Group, Advanced Institute of Materials Science, Ton Duc Thang University, Ho Chi Minh City 70000, Vietnam*

[4]*Faculty of Applied Sciences, Ton Duc Thang University, Ho Chi Minh City 70000, Vietnam*

(Received 14 September 2020; accepted 17 November 2020; published 4 December 2020)

For polar molecules, the degree of orientation is an essential variable with many interesting manifestations in strong-field phenomena. However, there is no direct way to measure the orientation degree in experiments. On the other hand, current indirect methods based on high-order harmonic generation (HHG) require specific laser conditions for characterization. In this study, we propose a general method to probe the whole range of orientation degrees by calibrating the time profile of harmonics. To develop the method, we first study the sensitivity of the harmonic time profile to the degree of orientation and then present a detailed procedure to extract this quantity from the harmonic time profile, which in turn is obtained from the HHG measurements. In our study, the "experimental" HHG data emitted from CO molecules are simulated by numerically solving the time-dependent Schrödinger equation. A strong point of the suggested method is its universal applicability with arbitrary laser pulse parameters. Moreover, not only the magnitude but also the sign of the degrees of orientation can be extracted accurately.

DOI: 10.1103/PhysRevA.102.063104

I. INTRODUCTION

High-order harmonic generation (HHG) from laser-matter interaction is one of the fastest-growing fields thanks to the recent revolution of attosecond science [1–6]. With the development of the alignment technique [7–9], HHG from prealigned molecules allows extracting molecular structures [10,11], reconstructing occupied molecular orbitals [12–15], and probing electron or nuclear dynamics in molecules [16–23]. In addition, the time-resolved HHG signals are implemented to measure the molecular alignment [24], as well as the rotational temperature and pump intensity [25,26], which control the alignment process.

Recently, many studies have been focused on asymmetric charged molecules because of their interesting effects in strong-field physics, such as the generation of both odd and even harmonics [27–32], multichannel emission of harmonics [33–36], large Stark effect [37], asymmetric ionization [38–40], or asymmetric HHG conversion efficiency [41–43]. For an assembly of such asymmetric molecules, besides the alignment, the orientation condition is especially important since now two opposite molecular orientations are nonequivalent. Until now, several orienting techniques have been developed, employing different fields, such as a strong dc field [44], a combination of a static electric field and a nonresonant femtosecond excitation [45,46], an electrostatic field combined with a nonresonant turned-off laser field [47], an IR and UV pulse pair [48], a THz pulse [49,50], or a two-color laser field [27,51–54]. By these methods, a high degree of orientation in asymmetric-molecule gas has been achieved.

However, a perfect orientation in experiments is infeasible. In this case, the degree of orientation is defined as the difference in the probabilities of the "head-versus-tail" molecules and the inversely oriented ones, the value of which ranges from -1 to $+1$ [28,29,55,56]. In fact, the knowledge of the orientation degree of an asymmetric-molecule sample is desirable and crucial in many physical and chemical processes. Nevertheless, this quantity cannot be directly measured in experiments [28,29]. To overcome this circumstance, several credible methods have been proposed to indirectly calculate the degree of orientation from experimental observations such as imaging fragment ion angular distributions after the induced-laser Coulomb explosion [45,52], or the free-induction decay [49,50].

Alternatively, from HHG one can also retrieve the degree of orientation of a molecular sample nondestructively by calibrating the HHG yield [56] or measuring the even-to-odd ratio [28,29,53,55]. However, the method of calibrating the HHG yield can only be used when a few-cycle laser pulse is chosen to interact with strongly polar molecules. This requirement for the laser pulse ensures its dramatic temporal change of the electric profile that leads to a significant difference in ionization and, consequently, in the HHG yield of oppositely oriented molecules [38,41]. Meanwhile, the application of the even-to-odd ratio is validated only when the laser duration is long enough that the odd and even harmonics are

*loanptn@hcmue.edu.vn

†Corresponding author: lethicamtu@tdtu.edu.vn

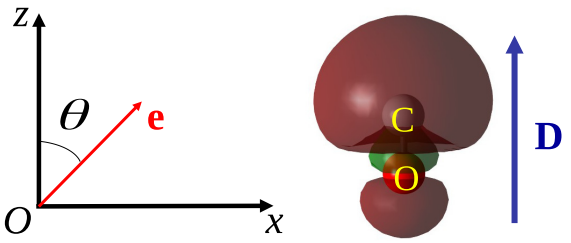

FIG. 1. The molecular frame Oxz of the CO molecule whose permanent dipole **D** is directed along the Oz axis. The electric field of the laser along the unit vector **e** makes an angle θ to the molecular axis.

clearly distinguishable [28,29,53,55]. Specifically, these even and odd harmonics are formed by the interference of coherent harmonic emissions bursting at successive half-cycles [28–30,32]. To secure this coherence, the pulse duration must be sufficiently long, i.e., a multicycle pulse, so that the electric magnitudes at every half optical cycle are almost identical. Besides, the method of using the even-to-odd ratio can probe only the magnitude but not the sign of the degree of orientation. In short, these two methods are applicable only for an appropriate laser with the pulse duration of either just few cycles, or many cycles.

In this paper we propose a general method to probe the whole range of degrees of orientation by HHG from a partially oriented sample of polar molecules. We demonstrate that a harmonic time profile emitted from CO molecules is sensitive to the degrees of orientation, regardless of the laser pulse shape and other laser parameters. Based on this fact, we then develop a procedure to probe degrees of orientation using the harmonic time profile that can be easily constructed from measuring both harmonic amplitudes and phases. With this procedure we show that the method can effectively detect not only magnitude but also the sign of the degree of orientation. Besides, the accuracy of the method is systematically studied by considering random errors of HHG measurements. For the method demonstration, we use the HHG that is numerically simulated by solving the time-dependent Schrödinger equation.

II. EFFECT OF ORIENTATION ON HHG SPECTRUM

We focus on an assembly of CO molecules with ideal alignment but possibly imperfect orientation. For this purpose, as presented in Fig. 1, we choose a coordinate system where the Oz axis coincides with the alignment axis. We differentiate two orientations along the Oz axis: parallel if the molecular permanent dipole points in the positive Oz direction and antiparallel if the dipole points in the negative Oz direction. Generically, a molecule after the orientation procedure can have a probability of P_u being parallel and P_d being antiparallel. Therefore the degree of orientation is defined as $\eta = P_u - P_d$, whose value ranges from -1 (for the sample with ideal antiparallel molecules) to $+1$ (for the sample with ideal parallel molecules). Here we choose the linearly polarized electric field (aligned along the unit vector **e** in Fig. 1), which makes an angle θ to the molecular axis. In this paper the alignment angle is $\theta = 0^\circ$ unless stated otherwise. We use the

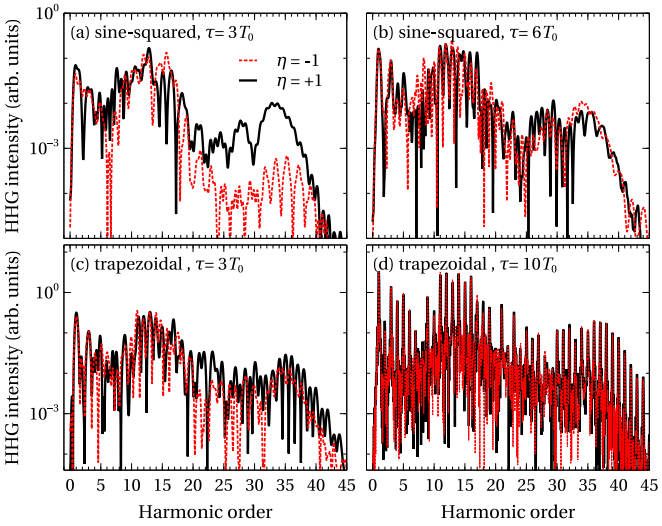

FIG. 2. The HHGs from CO molecules with $\eta = \pm 1$ exposed to different laser pulses. The pulses have the sine-squared (upper panels) and trapezoidal (lower panels) envelopes. The pulse duration is $3T_0$ [(a), (c)], $6T_0$ (b), and $10T_0$ (d), where T_0 is an optical cycle. The remaining laser parameters are $E_0 = 0.0755$ a.u., 800 nm, and CEP of π.

laser pulse with the wavelength of 800 nm, the peak amplitude $E_0 = 0.0755$ a.u., carrier-envelope phase (CEP) of π, and various pulse durations. The detailed method for calculating HHG is presented in detail in Appendix A.

In the following section, Sec. II A, we investigate the applicable range of the laser for the current methods of probing orientation degrees. Then, in Sec. II B, we demonstrate the asymmetry in the time-frequency spectrum and its sensitivity to the degree of orientation.

A. Applicable laser range of current methods for probing orientation degrees using HHG

To examine the applicable laser range of the current methods for probing the orientation degrees, we investigate the features of HHGs from oriented CO molecules illuminated by laser pulses with various parameters. We first present the HHGs in two limits $\eta = \pm 1$, i.e., the molecules are ideally oriented. The laser pulses with two forms of envelopes—sine-squared and trapezoidal—are used. We also vary the time duration of the laser pulse τ from 3 to 10 optical cycles.

Figure 2(a) indicates that in the three-cycle pulse with the sine-squared envelope, the HHGs contain two distinguishing plateaus. Interestingly, for the second HHG plateau, the two oppositely oriented samples have strikingly different conversion efficiency. Particularly, the HHG intensity of the $\eta = +1$ sample is about 1–2 orders of magnitude higher than that of $\eta = -1$ sample. This difference is the basis to utilize the second plateau's yield as a tool to probe the degree of orientation in Ref. [56]. Specifically, it demonstrates that the scaled intensity, i.e., the ratio of the second plateau's HHG intensity to that of an unoriented sample ($\eta = 0$), is a function of η. Thereby, the value of η can be extracted from the second plateau's yield.

However, this method is only valid if one uses a few-cycle pulse whose electric profile changes dramatically with time. As shown in Fig. 2(b), when using a six-cycle laser pulse, the second plateau's intensity for the two limits of orientation is no longer distinguishable. Our calculation shows that the distinguishability vanishes when the pulse with the number of optical cycles larger than 4 (not shown) is used. In addition, in Fig. 2(c) we demonstrate that the laser envelope also affects the ability to distinguish the plateaus in two limits $\eta = \pm 1$. With the three-cycle laser pulse, but the trapezoidal envelope, the HHG intensities at the two orientation limits are almost identical. In these cases the laser electric field is close to a steady harmonic oscillation in the middle of the pulse, and thus the ionization; consequently, the HHGs of opposite molecules are almost identical. Hence the HHG yield of polar molecules in such laser pulses cannot be used to probe the degrees of orientation. The stringent requirements of the HHG-yield calibrating method, i.e., few-cycle laser pulses and stabilized CEP, are achievable only by using state-of-the-art technology [57,58].

Instead, for multicycle laser pulses there is another method proposed in Refs. [28,29,53,55]. In multicycle pulses, such as a ten-cycle trapezoidal pulse shown in Fig. 2(d), besides the odd harmonics, the even ones also appear in the HHGs due to the symmetry breaking of the laser-molecule system. The works [28,29,53,55] have shown that the ratio between intensities of even and odd harmonics, referred to as the even-to-odd ratio, is proportional to the square of the orientation degree. However, this method requires the unambiguous manifestation of even and odd harmonics. For this reason the pulse has to be sufficiently long such that the magnitudes of half-cycle peaks are almost the same [28,29]. According to our investigation for the CO molecule, resolvable odd and even harmonics exist if the number of optical cycles is larger than about five for trapezoidal and about 25 for the sine-squared envelope. Additionally, it should be noted that the even-to-odd ratio allows detecting only the magnitude of η but not its sign.

In short, the above-mentioned methods of probing degrees of orientation using HHG can only be applied with certain constraints on the laser parameters. For lasers such as used in Figs. 2(b) and 2(c), both methods fail.

B. Asymmetry in time-frequency spectrum and its sensitivity to degrees of orientation

To gain some insight into developing our method, in this section we study the HHG at each emission time, i.e., the time-frequency spectrum of HHG. In fact, this profile is obtained via the time-frequency transform of the induced acceleration dipole $a(t)$. For this, we use in this paper the wavelet transform as

$$S(\omega, t) = \int_0^\tau a(t')\sqrt{\omega}W(\omega(t'-t))dt', \tag{1}$$

where ω is the harmonic frequency. The Morlet wavelet has the form $W(x) = (1/\sqrt{\sigma})e^{ix}e^{-x^2/2\sigma^2}$ [59,60]. By directly testing, we found that the time-frequency spectrum is stable for σ ranging from 5 to 30, which is consistent with Ref. [60]. Therefore, in this study we choose $\sigma = 20$. For theoretical investigation in this section, $a(t)$ is calculated by Eqs. (A6) and (A7) within the time-dependent Schrödinger equation (TDSE) method presented in Appendix A. For applying the method in reality, $a(t)$ can be constructed from the experimental harmonic intensity and phase, which is discussed in detail later.

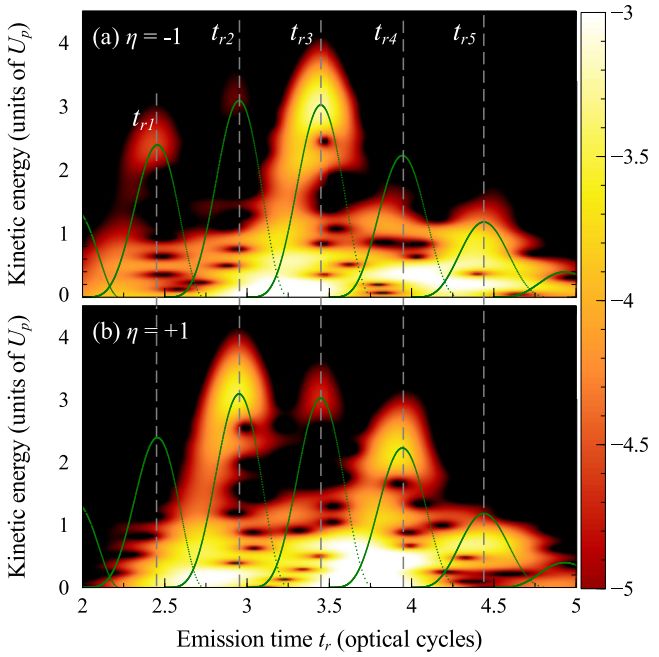

FIG. 3. The time-frequency spectrum obtained by TDSE for the CO-molecule samples with $\eta = -1$ (a) and $\eta = +1$ (b). The harmonic energy is presented as the equivalent kinetic energy (in the unit of the ponderomotive energy U_p) of the recombining electron upon the conversion law, i.e., $E_k = \omega - 1.3I_p$, where I_p is the ionization potential. The color bar is exhibited in the logarithm scale. The kinetic energy of the returning electron (green curves) is calculated by the classical approach. The vertical dashed lines indicate the emission times t_r of the emission peaks. The laser parameters are the same as used in Fig. 2(b). It is clear that for $\eta = -1$, the HHG mainly bursts at around t_{r1}, t_{r3}, and t_{r5}, while for $\eta = +1$, the HHG dominates at t_{r2} and t_{r4}.

Figure 3 presents the time-frequency analysis of HHG from the CO-molecule samples with $\eta = \pm 1$ obtained by the TDSE method. It also indicates the kinetic energy of the returning electron at the recombination time, obtained from the classical approach given in Appendix B. Here the sine-squared laser with the pulse duration $\tau = 6T_0$ is used, as in Fig. 2(b). The figures show that the two orientations $\eta = \pm 1$ separate the time-frequency spectra into two distinct patterns. Specifically, for $\eta = -1$, the bursts are predominantly produced at about half-integer multiples of the optical period. Meanwhile, for $\eta = +1$, the pattern shifts to about integer multiples of the optical period. These emission instants are entirely consistent with the classical simulation giving the maximum kinetic energy at $t_{r_1} = 2.45T_0$, $t_{r_3} = 3.45T_0$, $t_{r_5} = 4.44T_0$ for $\eta = -1$; and $t_{r2} = 2.95T_0$, $t_{r_4} = 3.94T_0$ for $\eta = +1$. It should be noticed that the HHG bursts for a given η are produced only once every full cycle of the driving laser, as shown in Fig. 3. This repetition for polar molecules totally differs from that

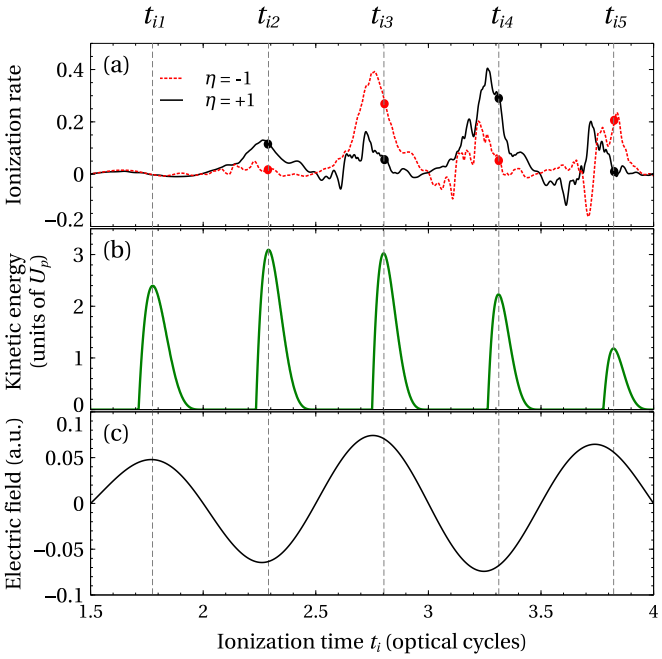

FIG. 4. The instantaneous ionization rates for the CO-molecule samples with $\eta = \pm 1$ (a). For convenience, the kinetic energy of the returning electron as a function of the ionization time (b) and the laser electric field (c) are also presented. The vertical dashed lines indicate the ionization instants t_i corresponding to the returning time t_r indicated in Fig. 3. For a clear illustration, the ionization rate is smoothed. The red and black circles indicate the ionization rates at the ionization time t_i. The laser parameters are the same as used in Fig. 2(b). Figure (a) indicates that the favorable orientation is alternated every half optical cycle.

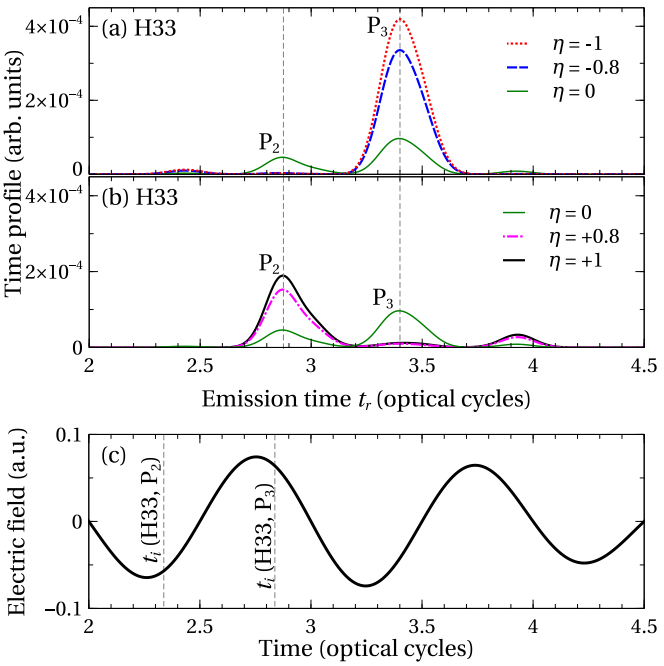

FIG. 5. The sensitivity of the time profile of the 33rd harmonic from a sample of CO molecules with different orientation degrees η (a), (b). The ionization instants of emission peaks P_2 and P_3 (c). The laser with parameters like those in Fig. 2(b) is used.

for atoms or symmetric molecules, where the emission bursts every half-cycle [61].

The asymmetry mentioned above of the time-frequency spectra has been well explained by considering the ionization probability in Refs. [38,41,56]. The authors claim that at the instants when the electric fields are antiparallel to the permanent dipole, the ionization enhances by raising the energy level of the dressed ground state. Vice versa, in the parallel case the dressed ground state is lowered, hence suppressing the tunneling strength. However, we realize that to explain the time-frequency spectrum, the amount of electron detached from molecules at each moment, i.e., the instantaneous ionization rate $\Gamma(t)$, is more relevant than the ionization probability $P(t)$, as proven in our previous studies [43,62]. Here $\Gamma(t)$ is directly derived from $P(t)$ as

$$\Gamma(t) = -\frac{d[\ln(1 - P(t))]}{dt}, \tag{2}$$

where $P(t)$ is calculated by Eq. (A5) in Appendix A. Therefore we suggest a more proper approach to explain the asymmetry of the time-frequency spectrum by the ionization rate as the following.

In Fig. 4(a) we show the ionization rate $\Gamma(t)$ for the CO samples with $\eta = \pm 1$. We also present the kinetic energy of the returning electron and the electric field in Figs. 4(b) and 4(c). According to Fig. 4(b), the HHG is mainly produced by the electron ionized around the time t_i (vertical dashed lines). Therefore we just focus on these instants. As shown in Fig. 4(a), at the instants t_{i2} and t_{i4}, $\Gamma(t)$ is stronger for the parallel orientation $\eta = +1$. This leads to the enhancement of the HHG bursts at the emission time t_{r2} and t_{r4}, as shown in Fig. 3(b). Meanwhile, for the antiparallel orientation $\eta = -1$, $\Gamma(t)$ predominates at t_{i1}, t_{i3}, and t_{i5}, which is consistent with the strong bursts at t_{r1}, t_{r3}, and t_{r5}, as exhibited in Fig. 3(a). The enhancement of $\Gamma(t)$ at t_{i2}, and t_{i4} for the case $\eta = +1$, is easily understood since, at these instants, the CO permanent dipole is antiparallel to the electric field, thus raising the laser-dressed ground state via the Stark effect. The same principle also applies to $\eta = -1$, but for the instants t_{i1}, t_{i3}, and t_{i5}. In other words, the ionization rate can completely describe the asymmetry of the time-frequency spectrum of the opposite-oriented CO molecules.

The asymmetry of the time-frequency spectra for $\eta = \pm 1$ suggests that it is sensitive to the orientation degree. For illustration, we show the time profile, i.e., the slice of a time-frequency spectrum at the 33rd harmonic (H33) for intermediate values of η in Figs. 5(a) and 5(b). The results indicate a strong dependence of the time profile on the orientation degrees. In particular, the position of emission instants for each harmonic is not affected by η, but the time-resolved HHG intensity varies strongly. This is a direct result of the nonoverlapping emission temporal patterns of the two opposite orientations, as exhibited in Fig. 3. Further investigation shows that the sensitivity to the degree of orientation always manifests in the time profile, regardless of the shape, wavelength, or intensity of the laser pulses (not shown).

III. DEGREE OF ORIENTATION CHARACTERIZATION

The sensitivity of the time profile offers a possibility of a general method to characterize the degrees of orientation from the HHG measurement. In this section we derive analytical formulas describing the relation between the harmonic time profile and the degree of orientation. These analytical expressions suggest a method to extract the orientation degree straightforwardly. It should be noted that practically, the fitting methods, i.e., one finds the set of parameters that, through a theoretical model, produces the best-fit data with the experimental one, can also be applied. We mention several successful fitting works to extract the molecular structures from HHG [63,64] or laser-induced electron diffraction [65–67]. Fitting methods necessitate a big database associating with a vast computational resource, particularly for complex systems, but sometimes are the best choice when there is no simple relation between the input and output. Fortunately, our analysis provides a direct connection between the degree of orientation and the time profile of HHG, which allows an analytical extraction method, rather than a fitting one.

A. Analytical expressions of time profile

Within the strong-field approximation [2,12,13,34], the HHG intensity from a molecule in an intense laser can be expressed as

$$S(\omega) = h(\omega)^2 |d(\omega)|^2. \tag{3}$$

Here $h(\omega) = N\omega^2 |c[k(\omega)]|$ is the spectral amplitude, where N is the number of produced ions; $c[k(\omega)]$ is the complex amplitude of the continuum state $|\mathbf{k}(\omega)\rangle$ with the wave number $k(\omega) = \sqrt{2(\omega - I_p)}$, where I_p is the ionization potential; and $d(\omega) = \langle \psi(\mathbf{r}, 0)| z |\mathbf{k}(\omega)\rangle$ is the transition dipole between the continuum $\mathbf{k}(\omega)$ and the HOMO state $\psi(\mathbf{r}, t = 0)$. This expression implies that the harmonic photon energy ω is mainly converted from the electron with kinetic energy $E_k = k(\omega)^2/2$. In fact, there are several trajectories (with different ionization and recombination instants) that produce the same electron kinetic energy upon recombination, thus leading to the overlapping in harmonics frequency [2]. Therefore we suppose that by taking the temporal-spectral profile one can separate these trajectories, i.e., the harmonic emission at t_r relevant to the electron ionization at t_i is

$$S(\omega, t_r) = h(\omega, t_i)^2 |d(\omega)|^2, \tag{4}$$

where $h(\omega, t_i)$ is the temporal-spectral amplitude.

For a sample of polar molecules with imperfect orientation, the averaged temporal-profile amplitude is written as

$$h(\omega, t_i) = P_u h_u(\omega, t_i) + P_d h_d(\omega, t_i), \tag{5}$$

in which $h_u(\omega, t_i)$, P_u and $h_d(\omega, t_i)$, P_d are the temporal-spectral amplitudes, and the probability of parallel and antiparallel molecules, respectively. We scale the time profile against one with random orientation, i.e., $P_u = P_d = 0.5$ or $\eta = 0$. It is called a scaled time profile and has the following form:

$$\frac{S(\omega, t_r)}{S_0(\omega, t_r)} = 4\left[\frac{P_u h_u(\omega, t_i) + P_d h_d(\omega, t_i)}{h_u(\omega, t_i) + h_d(\omega, t_i)}\right]^2. \tag{6}$$

At instants t_i, when the laser field reaches negative peaks, the ionization rate from parallel molecules dominates that from antiparallel molecules, thus $h_u(\omega, t_i) \gg h_d(\omega, t_i)$. As a consequence, Eq. (6) for the scaled time profile at t_r can be written as

$$\frac{S(\omega, t_r)}{S_0(\omega, t_r)} = 4P_u^2 = (1 + \eta)^2. \tag{7}$$

In this case, the scaled time profile has the form that is similar to the second plateau's yield calibration, as presented in Ref. [56]. The main difference is that we calibrate at a specific time-frequency point where the asymmetry always manifests strongly. On the other hand, in Ref. [56], the calibration is averaged over a range of frequency and time; as a result, the asymmetry effect might be canceled out if using multicycle laser pulses. In a similar manner, at the positive peaks of the electric field, $h_u(\omega, t_i) \ll h_d(\omega, t_i)$, leading to an alternative relation at the emission time t_r,

$$\frac{S(\omega, t_r)}{S_0(\omega, t_r)} = 4P_d^2 = (1 - \eta)^2. \tag{8}$$

Obviously, the scaled time profile in Eqs. (7) and (8) does not depend on the laser parameters. The two equations are different because they are used for different returning time t_r of electron ionized at different ionization time t_i. Specifically, Eq. (7) is applied when the ionization time t_i is near a negative peak of the laser pulse, while Eq. (8) is for t_i near a positive electric peak.

Formulas (7) and (8) are derived upon the strong-field approximation; thus their validity needs to be verified. For this purpose, we simulate the scaled time profile, i.e., the left-hand side of Eqs. (7) and (8), by the TDSE method. Particularly, the time profile $S(\omega, t_r)$ is constructed by Eq. (1), where $a(t)$ is calculated by the TDSE method. For the demonstration we simulate the time profile for H33 and present in Figs. 5(a) and 5(b). From these plots the emission instants t_r are easily defined. It should be noted that H33 bursts four times at different instants. We choose the two most prominent peaks emitted at instants P_2 and P_3, and scale the peak intensity against a sample with random orientation $\eta = 0$. Their scaled time profile is plotted by points in Fig. 6(a) for each given degree of orientation η. Besides, for comparison, the theoretical expectation, i.e., the right-hand sides of Eqs. (7) and (8), is also illustrated by the solid and black dashed lines.

Figure 6(a) shows a considerable consistency between the scaled time profile of peaks P_2 and P_3 of H33, and the theoretical expectation. In particular, the scaled time profile emitted at (H33, P_2) matches $(1 + \eta)^2$, i.e., Eq. (7). Meanwhile, the (H33, P_3) scaled time profile agrees with $(1 - \eta)^2$, i.e., Eq. (8). These results are easily understood by considering the ionization time t_i, which is derived from the knowing emission time t_r by the classical simulation presented in Appendix B. Specifically, as shown in Fig. 5(c), the ionization time t_i(H33, P_2) is close to a negative electric-field peak, and t_i(H33, P_3) is close to a positive electric-field peak. As a result, one expects Eq. (7) to hold for the scaled time profile at (H33, P_2) and Eq. (8) for a (H33, P_3) scaled time profile.

In principle, we can use either Eq. (7) or Eq. (8) to extract the orientation degree. However, Fig. 6(a) shows that the TDSE data are well consistent with Eq. (7) only for $\eta > -0.7$

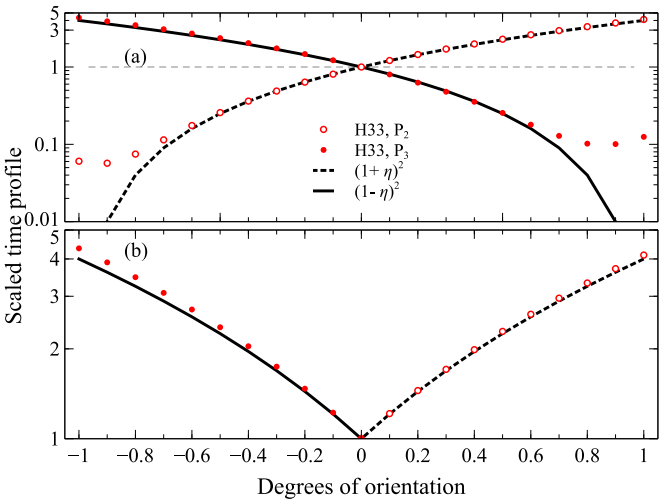

FIG. 6. The scaled time profile (points) for H33, calculated by the TDSE method, as a function of the degrees of orientation for CO molecules. The theoretical prediction (solid and black dashed lines) is also presented for comparison. The gray dashed line shows the scaled time profile equal to 1. The laser parameters are the same as in Fig. 2(b). The results show that for the scaled intensity larger than 0.1, the harmonic scaled time profile well matches the theoretical predictions Eqs. (7) and (8). The compact presentation with scaled time profile larger than 1 is exhibited in (b).

and with Eq. (8) only for $\eta < +0.7$. In other words, the consistency is satisfied for a moderate- and high-scaled time profile (>0.1). For a very low scaled time profile (<0.1), we observe a significant deviation. This is because the error caused by the unfavorable orientation is now comparable to the data value. In practice, a measured value that is too low is not reliable either, as it might also be affected by noise. Therefore, to ensure accurately probing the whole range of orientation degrees, we recommend our method for a moderate- or high-scaled time profile, ideally larger than 1; consequently, both Eqs. (7) and (8) are used. This means Eq. (7) is applied for the sample where parallel molecules are the majority, or $\eta > 0$, and vice versa, Eq. (8) for $\eta < 0$. Thereby, the compact illustration is presented in Fig. 6(b), where only a scaled time profile larger than 1 is used, which indicates consistency between the scaled time profile of a harmonic calculated by TDSE and the analytical prediction in the whole range of degrees of orientation. Besides, this agreement is satisfied not only for H33 but also for other harmonics (not shown). However, we note that harmonics with too low energy should not be taken, since their trajectories due to multiple rescatterings might disturb the validity of the analytical expressions.

B. Degree of orientation extraction procedure

This section presents a detailed procedure to apply the method for probing the orientation degree from experimental measurements. In experiments, the time profile harmonic intensity can be easily reconstructed from the HHG amplitude and HHG phase, which is commonly measured by RABITT (the reconstruction of attosecond beating by interference of two-photon transitions) [68–70] or FROG-CRAB (frequency-resolved optical gating for complete reconstruction of attosecond bursts) [6,71] methods. Then the dipole acceleration of the molecular sample is calculated by the inverse Fourier transform of the measured HHG, including amplitude and phase, as the following:

$$a(t) \propto \int \sqrt{I(\omega)} e^{i\Phi(\omega)} e^{-i\omega t} d\omega, \tag{9}$$

where $I(\omega)$ and $\Phi(\omega)$ are the harmonic intensity and phase, respectively. After that, the time-profile intensity can be obtained by using the time-frequency transform, such as the wavelet transform in Eq. (1). We notice that to obtain the scaled time profile, the experimental spectrum for the molecular sample with random orientation is also required.

Next, the time profile of a selected harmonic is plotted to determine the two pronounced emission peaks and corresponding emission time t_r. Then their time-profile intensity is calibrated against that of a sample with random orientation. Finally, the scaled time profile is compared to the analytical expressions Eqs. (7) and (8) to compute the degree of orientation. We remember that to determine which analytical expression is used, one relies on the electric field's direction at the ionization instants t_i, i.e., Eq. (8) if the electric field is positive and Eq. (7) if the electric field is negative at the ionization time. The relation between the emission time t_r and ionization time t_i can be easily deduced by the classical approach presented in Appendix. B.

We note that according to Eq. (9), in principle, the integral takes the whole range of harmonic frequency, i.e., from zero to the frequency at cutoff. But in fact, the full range of harmonics is not necessary to get the exact time-frequency spectrum. We carry out the reconstruction of the time profile of H33 from the full range of harmonics and from only nine harmonics around H33. The results show a complete convergence between the two cases (not shown). Consequently, in experiments, a narrow window of harmonics frequency is sufficient to compute the converged time-frequency spectrum.

C. General applicability of the method

We now verify the general applicability of the method mentioned above to retrieve the degree of orientation from HHG from polar molecules exposed to a laser with different laser parameters. Since the relevant experimental data for polar molecules are not readily available, we generate the "experimental" HHG intensity $I(\omega)$ and phase $\Phi(\omega)$ by the TDSE method for each "input" orientation degree η of the CO-molecule sample. We note that the above TDSE simulation only captures the microscopic single-molecule response. To incorporate macroscopic propagation, one can solve Maxwell's wave equations [72], which leads to the washout of the long trajectories signal due to their strong phase dependence on the laser intensity [24,72,73]. Therefore one way to artificially mimic phase matching is to remove the long trajectories by the coherent intensity averaging [74], or by filtering out the long trajectories in simulation [75]. In our TDSE calculation, we remove the contribution of the long trajectories by setting the absorbing boundary at the maximal displacement of the electron short trajectories in the laser field, specifically, $1.2E_0/\omega_0^2$ [75], where E_0 and ω_0 are the

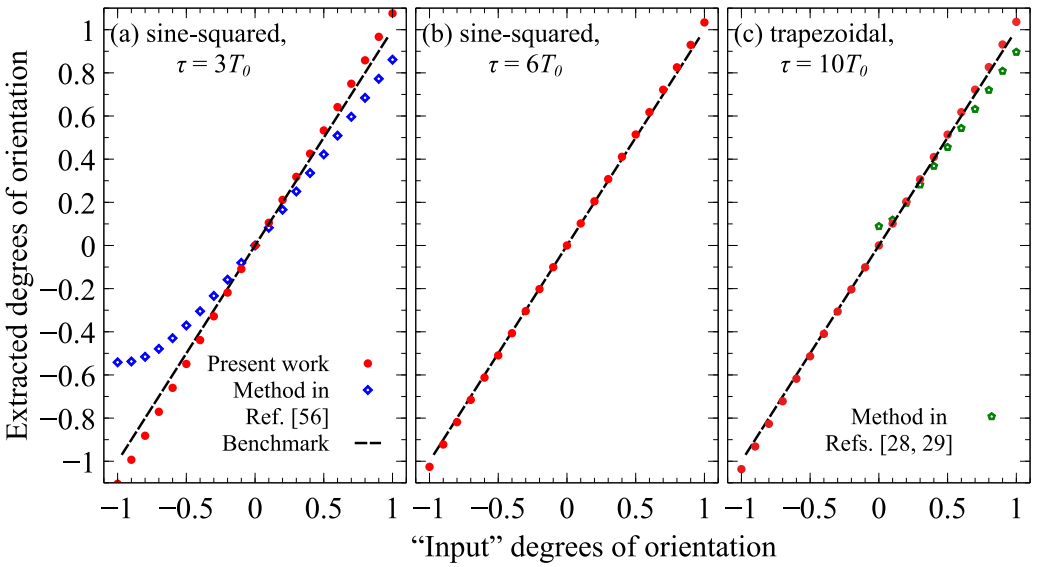

FIG. 7. The degrees of orientation extracted from the scaled time profile of harmonics calculated by the TDSE method for samples of CO molecules with diverse "input" orientation degrees for sine-squared lasers with $\tau = 3T_0$ (a), $\tau = 6T_0$ (b), and trapezoidal laser pulse with $\tau = 10T_0$ (c). The scaled time profiles are taken at H35 (a), H33 (b), and H36 (c). For comparison, the degrees of orientation detected by the method of calibrating the HHG yield in Ref. [56], and by the even-to-odd ratio as in Refs. [28,29], are also presented. The laser parameters are the same as in Fig. 2. The dashed lines show the exact results for the benchmark.

peak amplitude and the carrier frequency of the laser pulse. Even though our consideration of the macroscopic propagation might seem superficial, our method selects out a specific instant when only one trajectory contributes to most of the HHG, and the scaled time profile is thus relatively stable against the propagating condition.

After getting the "experimental" HHG, the scaled time profile is obtained by using Eqs. (9) and (1). Applying Eqs. (7) and (8), we infer the "extracted" degree of orientation and then compare it with the "input" one to estimate the method's systematic error.

The extracted degrees of orientation of the sample of CO molecules with varying "input" degrees of orientation interacting with the sine-squared laser pulse with $\tau = 3T_0$, $\tau = 6T_0$, and trapezoidal one with $\tau = 10T_0$ are presented in Fig. 7. The calculation is performed with the step of orientation degree of 0.1. For a clear illustration, some of the results are also exhibited in Table I. They indicate that the extracted orientation degrees are considerably consistent with the "input" ones with an average deviation of 7.8%, 2.2%, and 2.6% for three pulse-duration cases of $3T_0$, $6T_0$, and $10T_0$.

The validity range of this method is in contrast to the previous methods that upon the HHG yield validated only for a few-cycle pulse [56] or upon the even-to-odd ratio induced by a multicycle pulse [28,29,55]. Here, in Fig. 7 we demonstrate that the method using the scaled time profile not only gives a comparable accuracy but also overcomes the restrictions of applicable laser range of the previous methods. In Fig. 7(a) and Table I, for the few-cycle laser, the extracted results calculated by the method in Ref. [56] using our TDSE data are also presented. The results show that its accuracy, and that of our proposed method are comparable for $\eta > -0.4$. For the remaining region, the method based on the HHG yield causes large errors. The main reason is the omission of the

TABLE I. The extracted versus "input" degrees of orientation when using different laser pulses.

				Sine-squared, $\tau = 3T_0$					
"Input" η	−1	−0.8	−0.5	−0.2	0	0.2	0.5	0.8	1
Extracted η	−1.10	−0.88	−0.55	−0.22	0	0.21	0.53	0.86	1.08
Extracted η[a]	−0.54	−0.52	−0.37	−0.16	0	0.17	0.42	0.68	0.86
				Sine-squared, $\tau = 6T_0$					
"Input" η	−1	−0.8	−0.5	−0.2	0	0.2	0.5	0.8	1
Extracted η	−1.03	−0.82	−0.51	−0.20	0	0.20	0.51	0.83	1.03
				Trapezoidal, $\tau = 10T_0$					
"Input" η	−1	−0.8	−0.5	−0.2	0	0.2	0.5	0.8	1
Extracted η	−1.04	−0.83	−0.51	−0.20	0	0.20	0.51	0.83	1.04
Extracted η[b]					0.09	0.20	0.46	0.72	0.90

[a]Method in Ref. [56].
[b]Method in Refs. [28,29].

contribution of molecules parallel to the temporal electric field when their number is dominant.

For a multicycle laser pulse where the HHG contains clear odd and even harmonics, the degrees of orientation are a square root of the even-to-odd ratio [28,29,55]. Consequently, this method cannot distinguish the cases with the same degree of orientation but opposite signs. Therefore, in Fig. 7(c) and Table I we show the extracted orientation degree for only positive η. Meanwhile, the method based on the scaled time profile can detect not only the magnitude but also the sign of the degrees of orientation of the sample of polar molecules.

Besides the systematic error of the method, we also study the "random" error propagated from the experimental measurement of the harmonic intensity and phase. To examine the propagation of the HHG measurement errors to the extracted orientation degrees, we prepared "noisy" experimental data by seeding a random error to the HHG simulated by the TDSE method. Here we give an example for a sample of CO molecules with an "input" degree of orientation $\eta = 0.5$ exposed to the six-cycle sine-squared laser pulse. Then we include the random error of the harmonic intensity, which has a 95% confidence interval within $\pm 40\%$ of the expected value [69]. For the harmonic phase, the corresponding error interval is $\pm 20\%$ of the expected value [69]. From this "experimental" HHG, the "extracted" degree of orientation is retrieved by our proposed method. With our simulation, after the error propagation the extracted degree of orientation fluctuates at around $\eta = 0.517$ with the 95% confidence level of [0.459, 0.573]. We emphasize that the averaged value $\eta = 0.517$ is slightly deviated with the "extracted" degree of orientation when ignoring the random error, $\eta = 0.514$. This small dispersion demonstrates the stability of the extracted value despite the relatively large random error of the "experimental" HHG.

IV. CONCLUSION

In this paper we have studied in detail the asymmetry in the time-frequency spectrum of HHG from oppositely orientated polar molecules. Besides, we have also demonstrated the sensitivity of the harmonic time profile to the degree of orientation and then constructed an analytical expression describing the straightforward relation between the scaled time profile and the orientation degree. From these insights we have proposed a general method to probe the degree of orientation from the scaled time profile of HHG of polar molecules regardless of the laser parameters. For applying the method, a detailed procedure is presented.

The advantage of the proposed method is that it is not constrained to a particular regime of laser parameters. The used laser can have an arbitrary pulse shape, pulse duration, and the method can probe a whole range of degrees of orientation. We expect the same principle to be applicable also to imperfectly aligned samples. Such generalization will fully characterize a gas sample, which opens more possibilities in experiments. We are also interested in future experimental works that compare the orientation probing using the time profile of HHG with those using other phenomena.

ACKNOWLEDGMENTS

We are funded by the Program of Fundamental Research of the Ministry of Education and Training (Vietnam) under Grant No. B2019-SPS-06. This work was carried out by the high performance cluster at Ho Chi Minh City University of Education, Vietnam.

APPENDIX A: NUMERICAL METHOD

In this Appendix we present the method for numerically solving the TDSE [32,43,76] of the CO molecule in the laser pulse within the single-active-electron (SAE) model [77,78]. The detailed construction of the SAE potential for the CO molecule can be found in our previous studies [32,43,76]. The energy of the orbital 5σ of CO is -0.520 a.u., which is consistent with the experimental value of -0.514 a.u. [79]. Besides, the 5σ permanent dipole $D = 1.55$ a.u. well agrees with 1.57 a.u. calculated by the time-dependent density functional theory in Ref. [80].

The TDSE of the CO molecule in the laser pulse written in the atomic units ($\hbar = m_e = e = 1$) has the following form:

$$i\frac{\partial}{\partial t}\psi(\mathbf{r},t) = [\hat{H}_0 + V(\mathbf{r},t)]\psi(\mathbf{r},t). \tag{A1}$$

Here $\psi(\mathbf{r},t)$ is the wave function of the active electron with the coordinate $\mathbf{r}$. $\hat{H}_0 = -\nabla^2/2 + V_{\mathrm{SAE}}(\mathbf{r})$ is the field-free Hamiltonian with the SAE potential $V_{\mathrm{SAE}}(\mathbf{r})$.

The laser-induced potential $V(\mathbf{r},t)$ is

$$V(\mathbf{r},t) = \mathbf{r}\cdot\mathbf{E}(t) + V_p(\mathbf{r},t), \tag{A2}$$

where the first component is the interacting potential of the active electron with the electric field. The second one,

$$V_p(\mathbf{r},t) = -\frac{\mathbf{E}(t)\hat{\alpha}_c\mathbf{r}}{r^3}, \tag{A3}$$

presents the interaction between the active electron with the dynamic core-electron polarization induced by the laser field. Here $\hat{\alpha}_c$ is the total polarizability tensor of the core-electron system whose values for the CO molecule is taken from Ref. [40]. To avoid the singularity near the core, we apply the cutoff for V_p at the point r_c, where at $r \leqslant r_c$, the polarization field cancels the laser electric field [39,81]. We use a linearly polarized laser pulse whose electric field $\mathbf{E}(t)$ is given as

$$\mathbf{E}(t) = \mathbf{e}\, E_0 f(t)\sin(\omega_0 t + \varphi), \tag{A4}$$

where E_0, ω_0, and φ (chosen as π in the main text) are the peak amplitude, carrier frequency, and CEP of the laser, respectively. $f(t)$ is the envelope of the laser pulse.

To solve the Schrödinger equation (A1), we utilize the procedure giving in Refs. [32,43,76]. Accordingly, the time-dependent wave function is expanded into a linear combination of the field-free Hamiltonian $\hat{H}_0$ eigenfunctions. The time-dependent coefficients in this combination are numerically found by the fourth-order Runge-Kutta method in which the initial condition is that when the laser starts to interact with the molecule, the active electron is given in the highest occupied molecular orbital 5σ. All parameters for numerical simulation are checked to ensure the convergence.

After getting the time-dependent wave function, we calculate the ionization probability as

$$P(t) = 1 - \sum_{\substack{n,m \\ E_n^m < 0}} \langle \Phi_n^m(\mathbf{r}) | \psi(\mathbf{r}, t) \rangle , \tag{A5}$$

in which $\Phi_n^m(\mathbf{r})$ and E_n^m are respectively the eigenfunctions and eigenvalues of the states with quantum numbers n, m of the field-free Hamiltonian $\hat{H}_0$. The time-dependent dipole acceleration is defined as

$$\mathbf{a}(t) = \frac{d^2}{dt^2} \langle \psi(\mathbf{r}, t) | \mathbf{r} | \psi(\mathbf{r}, t) \rangle . \tag{A6}$$

For an assembly of polar molecules with partial orientation, the acceleration dipole is averaged as

$$a(t) = P_u a_u(t) + P_d a_d(t). \tag{A7}$$

Here $a_u(t)$ and $a_d(t)$ are the time-dependent acceleration dipoles of parallel and antiparallel molecules, respectively. The HHG spectra are calculated by taking the Fourier transform of the time-dependent acceleration dipole

$$I(\omega) \propto \left| \int_0^\tau \hat{\mathbf{n}} \cdot \mathbf{a}(t) e^{i\omega t} dt \right|^2 , \tag{A8}$$

where τ is the time duration of the laser pulse and $\hat{\mathbf{n}}$ is a unit vector. In this study we focus on analyzing the case of alignment angle $\theta = 0^\circ$. In this case only HHG with polarization $\hat{\mathbf{n}}$ parallel to the electric field exists, whereas the HHG with the polarization perpendicular to $\mathbf{E}(t)$ vanishes.

APPENDIX B: CLASSICAL TRAJECTORY

To investigate the motion of the electron in the continuum region, we utilize the classical approach, which is popularly presented in Refs. [2,82]. Accordingly, the electron is driven by the laser field, which is described by Newton's second law,

$$\ddot{z}(t) = -E(t), \tag{B1}$$

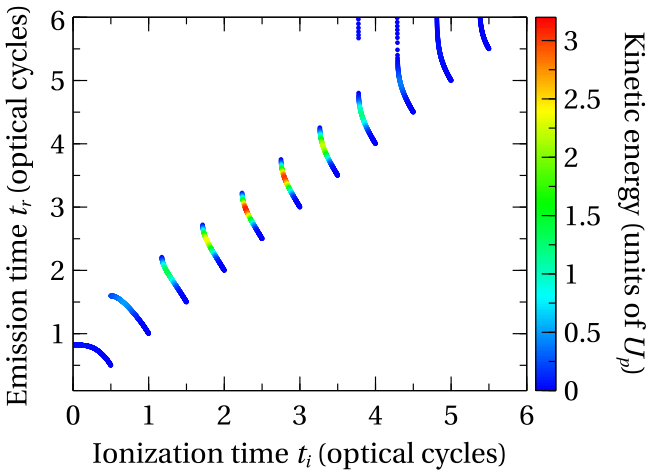

FIG. 8. The mapping of the recombination time t_r and the ionization time t_i. The color represents the kinetic energy of the electron at the returning time t_r. The laser parameters are the same as in Fig. 2(b).

where $z(t)$ is the trajectory of the electron. To solve this equation, the initial conditions are required. We assume that the electron ionizes at the origin with zero velocity, i.e., $z(t_i) = 0$ and $\dot{z}(t_i) = 0$.

At the recombination time t_r, the electron revisits the parent ion $z(t_r) = 0$ with the accumulated kinetic energy $E_k = \dot{z}^2(t_r)/2$. This energy is converted to the HHG photon with energy conservation $\omega = 1.3I_p + E_k$. It is worth noting that due to the effects of quantum tunneling and quantum diffusion [2], this cutoff law slightly differs from the conventional form $\omega = I_p + E_k$.

The correlation between the recombination time t_r and ionization time t_i, and the corresponding kinetic energy of the returning electron are illustrated in Fig. 8. Thereby, from the knowledge of the emission time t_r of a fixed harmonic ω, which is converted from the kinetic energy E_k of the returning electron, we can easily infer the ionization instant t_i.

[1] P. B. Corkum, Plasma Perspective on Strong Field Multiphoton Ionization, Phys. Rev. Lett. **71**, 1994 (1993).

[2] M. Lewenstein, P. Balcou, M. Y. Ivanov, A. L'Huillier, and P. B. Corkum, Theory of high-harmonic generation by low-frequency laser fields, Phys. Rev. A **49**, 2117 (1994).

[3] K. Zhao, Q. Zhang, M. Chini, Y. Wu, X. Wang, and Z. Chang, Tailoring a 67 attosecond pulse through advantageous phase-mismatch, Opt. Lett. **37**, 3891 (2012).

[4] J. Li, X. Ren, Y. Yin, K. Zhao, A. Chew, Y. Cheng, E. Cunningham, Y. Wang, S. Hu, Y. Wu, M. Chini, and Z. Chang, 53-attosecond X-ray pulses reach the carbon K-edge, Nat. Commun. **8**, 186 (2017).

[5] T. Gaumnitz, A. Jain, Y. Pertot, M. Huppert, I. Jordan, F. Ardana-Lamas, and H. J. Wörner, Streaking of 43-attosecond soft-X-ray pulses generated by a passively CEP-stable mid-infrared driver, Opt. Express **25**, 27506 (2017).

[6] Z. Yang, W. Cao, X. Chen, J. Zhang, Y. Mo, H. Xu, K. Mi, Q. Zhang, P. Lan, and P. Lu, All-optical frequency-resolved optical gating for isolated attosecond pulse reconstruction, Opt. Lett. **45**, 567 (2020).

[7] H. Stapelfeldt and T. Seideman, Colloquium: Aligning molecules with strong laser pulses, Rev. Mod. Phys. **75**, 543 (2003).

[8] M. Leibscher, I. S. Averbukh, and H. Rabitz, Molecular Alignment by Trains of Short Laser Pulses, Phys. Rev. Lett. **90**, 213001 (2003).

[9] A. S. Chatterley, C. Schouder, L. Christiansen, B. Shepperson, M. H. Rasmussen, and H. Stapelfeldt, Long-lasting field-free alignment of large molecules inside helium nanodroplets, Nat. Commun. **10**, 133 (2019).

[10] M. Lein, N. Hay, R. Velotta, J. P. Marangos, and P. L. Knight, Interference effects in high-order harmonic generation with molecules, Phys. Rev. A **66**, 023805 (2002).

[11] H. J. Wörner, J. B. Bertrand, P. Hockett, P. B. Corkum, and D. M. Villeneuve, Controlling the Interference of Multiple

Molecular Orbitals in High-Harmonic Generation, Phys. Rev. Lett. **104**, 233904 (2010).

[12] J. Itatani, J. Levesque, D. Zeidler, H. Niikura, H. Pépin, J.-C. Kieffer, P. B. Corkum, and D. M. Villeneuve, Tomographic imaging of molecular orbitals, Nature (London) **432**, 867 (2004).

[13] V.-H. Le, A.-T. Le, R.-H. Xie, and C. D. Lin, Theoretical analysis of dynamic chemical imaging with lasers using high-order harmonic generation, Phys. Rev. A **76**, 013414 (2007).

[14] Y. J. Chen, L. B. Fu, and J. Liu, Asymmetric Molecular Imaging through Decoding Odd-Even High-Order Harmonics, Phys. Rev. Lett. **111**, 073902 (2013).

[15] C. Zhai, X. Zhu, P. Lan, F. Wang, L. He, W. Shi, Y. Li, M. Li, Q. Zhang, and P. Lu, Diffractive molecular-orbital tomography, Phys. Rev. A **95**, 033420 (2017).

[16] O. Smirnova, Y. Mairesse, S. Patchkovskii, N. Dudovich, D. Villeneuve, P. Corkum, and M. Y. Ivanov, High harmonic interferometry of multi-electron dynamics in molecules, Nature (London) **460**, 972 (2009).

[17] S. Haessler, J. Caillat, W. Boutu, C. Giovanetti-Teixeira, T. Ruchon, T. Auguste, Z. Diveki, P. Breger, A. Maquet, B. Carré, R. Taïeb, and P. Salières, Attosecond imaging of molecular electronic wavepackets, Nat. Phys. **6**, 200 (2010).

[18] P. M. Kraus, B. Mignolet, D. Baykusheva, A. Rupenyan, L. Horný, E. F. Penka, G. Grassi, O. I. Tolstikhin, J. Schneider, F. Jensen, L. B. Madsen, A. D. Bandrauk, F. Remacle, and H. J. Wörner, Measurement and laser control of attosecond charge migration in ionized iodoacetylene, Science **350**, 790 (2015).

[19] H. J. Wörner, C. A. Arrell, N. Banerji, A. Cannizzo, M. Chergui, A. K. Das, P. Hamm, U. Keller, P. M. Kraus, E. Liberatore, P. Lopez-Tarifa, M. Lucchini, M. Meuwly, C. Milne, J.-E. Moser, U. Rothlisberger, G. Smolentsev, J. Teuscher, J. A. van Bokhoven, and O. Wenger, Charge migration and charge transfer in molecular systems, Struct. Dyn. **4**, 061508 (2017).

[20] M. Lein, Attosecond Probing of Vibrational Dynamics with High-Harmonic Generation, Phys. Rev. Lett. **94**, 053004 (2005).

[21] S. Baker, J. S. Robinson, M. Lein, C. C. Chirilă, R. Torres, H. C. Bandulet, D. Comtois, J. C. Kieffer, D. M. Villeneuve, J. W. G. Tisch, and J. P. Marangos, Dynamic Two-Center Interference in High-Order Harmonic Generation from Molecules with Attosecond Nuclear Motion, Phys. Rev. Lett. **101**, 053901 (2008).

[22] P. Lan, M. Ruhmann, L. He, C. Zhai, F. Wang, X. Zhu, Q. Zhang, Y. Zhou, M. Li, M. Lein, and P. Lu, Attosecond Probing of Nuclear Dynamics with Trajectory-Resolved High-Harmonic Spectroscopy, Phys. Rev. Lett. **119**, 033201 (2017).

[23] P. Peng, C. Marceau, and D. M. Villeneuve, Attosecond imaging of molecules using high harmonic spectroscopy, Nat. Rev. Phys. **1**, 144 (2019).

[24] C. Jin, S.-J. Wang, S.-F. Zhao, A.-T. Le, and C. D. Lin, Robust control of the minima of high-order harmonics by fine-tuning the alignment of CO_2 molecules for shaping attosecond pulses and probing molecular alignment, Phys. Rev. A **102**, 013108 (2020).

[25] K. Yoshii, G. Miyaji, and K. Miyazaki, Measurement of molecular rotational temperature in a supersonic gas jet with high-order harmonic generation, Opt. Lett. **34**, 1651 (2009).

[26] Y. He, L. He, P. Wang, B. Wang, S. Sun, R. Liu, B. Wang, P. Lan, and P. Lu, Measuring the rotational temperature and pump intensity in molecular alignment experiments via high harmonic generation, Opt. Express **28**, 21182 (2020).

[27] P. M. Kraus, A. Rupenyan, and H. J. Wörner, High-Harmonic Spectroscopy of Oriented OCS Molecules: Emission of Even and Odd Harmonics, Phys. Rev. Lett. **109**, 233903 (2012).

[28] E. Frumker, N. Kajumba, J. B. Bertrand, H. J. Wörner, C. T. Hebeisen, P. Hockett, M. Spanner, S. Patchkovskii, G. G. Paulus, D. M. Villeneuve, A. Naumov, and P. B. Corkum, Probing Polar Molecules with High Harmonic Spectroscopy, Phys. Rev. Lett. **109**, 233904 (2012).

[29] E. Frumker, C. T. Hebeisen, N. Kajumba, J. B. Bertrand, H. J. Wörner, M. Spanner, D. M. Villeneuve, A. Naumov, and P. B. Corkum, Oriented Rotational Wave-Packet Dynamics Studies via High Harmonic Generation, Phys. Rev. Lett. **109**, 113901 (2012).

[30] H. Hu, N. Li, P. Liu, R. Li, and Z. Xu, Pure Even Harmonic Generation from Oriented CO in Linearly Polarized Laser Fields, Phys. Rev. Lett. **119**, 173201 (2017).

[31] J. Heslar, D. A. Telnov, and S.-I. Chu, Generation of circularly polarized XUV and soft-x-ray high-order harmonics by homonuclear and heteronuclear diatomic molecules subject to bichromatic counter-rotating circularly polarized intense laser fields, Phys. Rev. A **96**, 063404 (2017).

[32] N.-L. Phan, C.-T. Le, V.-H. Hoang, and V.-H. Le, Odd–even harmonic generation from oriented CO molecules in linearly polarized laser fields and the influence of the dynamic core-electron polarization, Phys. Chem. Chem. Phys. **21**, 24177 (2019).

[33] X.-B. Bian and A. D. Bandrauk, Multichannel Molecular High-Order Harmonic Generation from Asymmetric Diatomic Molecules, Phys. Rev. Lett. **105**, 093903 (2010).

[34] Y. Chen and B. Zhang, Tracing the structure of asymmetric molecules from high-order harmonic generation, Phys. Rev. A **84**, 053402 (2011).

[35] X.-Y. Miao and H.-N. Du, Theoretical study of high-order-harmonic generation from asymmetric diatomic molecules, Phys. Rev. A **87**, 053403 (2013).

[36] X. Xie, S. Yu, W. Li, S. Wang, and Y. Chen, Routes of odd-even harmonic emission from oriented polar molecules, Opt. Express **26**, 18578 (2018).

[37] A. Etches and L. B. Madsen, Extending the strong-field approximation of high-order harmonic generation to polar molecules: Gating mechanisms and extension of the harmonic cutoff, J. Phys. B: At. Mol. Opt. **43**, 155602 (2010).

[38] G. L. Kamta and A. D. Bandrauk, Phase Dependence of Enhanced Ionization in Asymmetric Molecules, Phys. Rev. Lett. **94**, 203003 (2005).

[39] B. Zhang, J. Yuan, and Z. Zhao, Dynamic Core Polarization in Strong-Field Ionization of CO Molecules, Phys. Rev. Lett. **111**, 163001 (2013).

[40] V.-H. Hoang, S.-F. Zhao, V.-H. Le, and A.-T. Le, Influence of permanent dipole and dynamic core-electron polarization on tunneling ionization of polar molecules, Phys. Rev. A **95**, 023407 (2017).

[41] G. L. Kamta, A. D. Bandrauk, and P. B. Corkum, Asymmetry in the harmonic generation from nonsymmetric molecules, J. Phys. B: At. Mol. Opt, **38**, L339 (2005).

[42] B. Zhang, J. Yuan, and Z. Zhao, Dynamic orbitals in high-order harmonic generation from CO molecules, Phys. Rev. A **90**, 035402 (2014).

[43] C.-T. Le, V.-H. Hoang, L.-P. Tran, and V.-H. Le, Effect of the dynamic core-electron polarization of CO molecules on high-order harmonic generation, Phys. Rev. A **97**, 043405 (2018).

[44] B. Friedrich and D. R. Herschbach, Spatial orientation of molecules in strong electric fields and evidence for pendular states, Nature (London) **353**, 412 (1991).

[45] H. Sakai, S. Minemoto, H. Nanjo, H. Tanji, and T. Suzuki, Controlling the Orientation of Polar Molecules with Combined Electrostatic and Pulsed, Nonresonant Laser Fields, Phys. Rev. Lett. **90**, 083001 (2003).

[46] O. Ghafur, A. Rouzée, A. Gijsbertsen, W. K. Siu, S. Stolte, and M. J. Vrakking, Impulsive orientation and alignment of quantum-state-selected NO molecules, Nat. Phys. **5**, 289 (2009).

[47] A. Goban, S. Minemoto, and H. Sakai, Laser-Field-Free Molecular Orientation, Phys. Rev. Lett. **101**, 013001 (2008).

[48] A. V. Sokolov, K. K. Lehmann, M. O. Scully, and D. Herschbach, Orienting molecules via an IR and UV pulse pair: Implications for coherent Raman spectroscopy, Phys. Rev. A **79**, 053805 (2009).

[49] S. Fleischer, Y. Zhou, R. W. Field, and K. A. Nelson, Molecular Orientation and Alignment by Intense Single-Cycle THz Pulses, Phys. Rev. Lett. **107**, 163603 (2011).

[50] P. Babilotte, K. Hamraoui, F. Billard, E. Hertz, B. Lavorel, O. Faucher, and D. Sugny, Observation of the field-free orientation of a symmetric-top molecule by terahertz laser pulses at high temperature, Phys. Rev. A **94**, 043403 (2016).

[51] M. J. Vrakking and S. Stolte, Coherent control of molecular orientation, Chem. Phys. Lett. **271**, 209 (1997).

[52] S. De, I. Znakovskaya, D. Ray, F. Anis, N. G. Johnson, I. A. Bocharova, M. Magrakvelidze, B. D. Esry, C. L. Cocke, I. V. Litvinyuk, and M. F. Kling, Field-Free Orientation of CO Molecules by Femtosecond Two-Color Laser Fields, Phys. Rev. Lett. **103**, 153002 (2009).

[53] P. M. Kraus, D. Baykusheva, and H. J. Wörner, Two-pulse orientation dynamics and high-harmonic spectroscopy of strongly-oriented molecules, J. Phys. B: At. Mol. Opt. **47**, 124030 (2014).

[54] J. H. Mun, H. Sakai, and R. González-Férez, Orientation of linear molecules in two-color laser fields with perpendicularly crossed polarizations, Phys. Rev. A **99**, 053424 (2019).

[55] S. J. Yu, W. Y. Li, Y. P. Li, and Y. J. Chen, Probing degrees of orientation of top molecules with odd-even high-order harmonics, Phys. Rev. A **96**, 013432 (2017).

[56] Y. Z. Shi, B. Zhang, W. Y. Li, S. J. Yu, and Y. J. Chen, Probing degrees of orientation of polar molecules with harmonic emission in ultrashort laser pulses, Phys. Rev. A **95**, 033406 (2017).

[57] W. Cao, P. Lu, P. Lan, X. Wang, and G. Yang, Single-attosecond pulse generation with an intense multicycle driving pulse, Phys. Rev. A **74**, 063821 (2006).

[58] P. Lan, P. Lu, W. Cao, X. Wang, and W. Hong, Single attosecond pulse generation from asymmetric molecules with a multicycle laser pulse, Opt. Lett. **32**, 1186 (2007).

[59] X.-M. Tong and S.-I. Chu, Probing the spectral and temporal structures of high-order harmonic generation in intense laser pulses, Phys. Rev. A **61**, 021802(R) (2000).

[60] X. Chu and S.-I. Chu, Self-interaction-free time-dependent density-functional theory for molecular processes in strong fields: High-order harmonic generation of H_2 in intense laser fields, Phys. Rev. A **63**, 023411 (2001).

[61] P. Antoine, A. L'Huillier, and M. Lewenstein, Attosecond Pulse Trains Using High-Order Harmonics, Phys. Rev. Lett. **77**, 1234 (1996).

[62] N.-L. Phan, T.-T. Nguyen, H. Mineo, and V.-H. Hoang, Depletion effect in high-order harmonic generation with coherent superposition state, J. Opt. Soc. Am. B **37**, 311 (2020).

[63] V.-H. Le, N.-T. Nguyen, C. Jin, A.-T. Le, and C. D. Lin, Retrieval of interatomic separations of molecules from laser-induced high-order harmonic spectra, J. Phys. B: At. Mol. Opt. **41**, 085603 (2008).

[64] R. M. Lock, S. Ramakrishna, X. Zhou, H. C. Kapteyn, M. M. Murnane, and T. Seideman, Extracting Continuum Electron Dynamics from High Harmonic Emission from Molecules, Phys. Rev. Lett. **108**, 133901 (2012).

[65] C. I. Blaga, J. Xu, A. D. DiChiara, E. Sistrunk, K. Zhang, P. Agostini, T. A. Miller, L. F. DiMauro, and C. Lin, Imaging ultrafast molecular dynamics with laser-induced electron diffraction, Nature (London) **483**, 194 (2012).

[66] B. Wolter, M. G. Pullen, A.-T. Le, M. Baudisch, K. Doblhoff-Dier, A. Senftleben, M. Hemmer, C. D. Schröter, J. Ullrich, T. Pfeifer, R. Moshammer, S. Gräfe, O. Vendrell, C. D. Lin, and J. Biegert, Ultrafast electron diffraction imaging of bond breaking in di-ionized acetylene, Science **354**, 308 (2016).

[67] D.-D. T. Vu, N.-L. T. Phan, V.-H. Hoang, and V.-H. Le, Dynamic molecular structure retrieval from low-energy laser-induced electron diffraction spectra, J. Phys. B: At. Mol. Opt. **50**, 245101 (2017).

[68] P. M. Paul, E. S. Toma, P. Breger, G. Mullot, F. Augé, P. Balcou, H. G. Muller, and P. Agostini, Observation of a train of attosecond pulses from high harmonic generation, Science **292**, 1689 (2001).

[69] A. Rupenyan, J. B. Bertrand, D. M. Villeneuve, and H. J. Wörner, All-Optical Measurement of High-Harmonic Amplitudes and Phases in Aligned Molecules, Phys. Rev. Lett. **108**, 033903 (2012).

[70] J. Mauritsson, P. Johnsson, E. Gustafsson, A. L'Huillier, K. J. Schafer, and M. B. Gaarde, Attosecond Pulse Trains Generated Using Two Color Laser Fields, Phys. Rev. Lett. **97**, 013001 (2006).

[71] Y. Mairesse and F. Quéré, Frequency-resolved optical gating for complete reconstruction of attosecond bursts, Phys. Rev. A **71**, 011401(R) (2005).

[72] C. Jin, A.-T. Le, and C. D. Lin, Retrieval of target photorecombination cross sections from high-order harmonics generated in a macroscopic medium, Phys. Rev. A **79**, 053413 (2009).

[73] F. Lindner, W. Stremme, M. G. Schätzel, F. Grasbon, G. G. Paulus, H. Walther, R. Hartmann, and L. Strüder, High-order harmonic generation at a repetition rate of 100 kHz, Phys. Rev. A **68**, 013814 (2003).

[74] A.-T. Le, T. Morishita, and C. D. Lin, Extraction of the species-dependent dipole amplitude and phase from high-order harmonic spectra in rare-gas atoms, Phys. Rev. A **78**, 023814 (2008).

[75] S. Yu, B. Zhang, Y. Li, S. Yang, and Y. Chen, Ellipticity of odd-even harmonics from oriented asymmetric molecules in strong linearly polarized laser fields, Phys. Rev. A **90**, 053844 (2014).

[76] C.-T. Le, D.-D. Vu, C. Ngo, and V.-H. Le, Influence of dynamic core-electron polarization on the structural minimum in high-order harmonics of CO_2 molecules, Phys. Rev. A **100**, 053418 (2019).

[77] M. Abu-samha and L. B. Madsen, Single-active-electron potentials for molecules in intense laser fields, Phys. Rev. A **81**, 033416 (2010).

[78] S.-F. Zhao, C. Jin, A.-T. Le, T. F. Jiang, and C. D. Lin, Determination of structure parameters in strong-field tunneling ionization theory of molecules, Phys. Rev. A **81**, 033423 (2010).

[79] K. Siegbahn, Electron spectroscopy — An outlook, J. Electron Spectros. Relat. Phenom. **5**, 3 (1974).

[80] J. Heslar, D. Telnov, and S.-I. Chu, High-order-harmonic generation in homonuclear and heteronuclear diatomic molecules: Exploration of multiple orbital contributions, Phys. Rev. A **83**, 043414 (2011).

[81] Z. Zhao and T. Brabec, Tunnel ionization in complex systems, J. Mod. Opt **54**, 981 (2007).

[82] G. G. Paulus, W. Becker, W. Nicklich, and H. Walther, Rescattering effects in above-threshold ionization: A classical model, J. Phys. B: At. Mol. Opt. **27**, L703 (1994).